Perovskite solar cells prepared by advanced Three-step method using additional $HC(NH_2)_2I$ spin-coating: efficiency improvement with multiple bandgap structure

Yuji Okamoto[†], Takeshi Yasuda[‡], Masatomo Sumiya[§] and Yoshikazu Suzuki[*, ∥]

[†]Graduate School of Pure and Applied Sciences, University of Tsukuba, 1-1-1 Tennodai, Tsukuba, Ibaraki 305-8573, Japan.

[‡]Research Center for Functional Materials, National Institute for Materials Science (NIMS), 1-2-1 Sengen, Tsukuba 305-0047, Japan.

[§]Widegap Materials group, National Institute for Materials Science (NIMS), 1-1 Namiki, Tsukuba, Ibaraki 305-0044, Japan.

[∥]Faculty of Pure and Applied Sciences, University of Tsukuba, 1-1-1 Tennodai, Tsukuba, Ibaraki 305-8573, Japan.

ABSTRACT

In the conventional 2-step prepared perovskite solar cells, the $CH_3NH_3PbI_3$ ($MAPbI_3$) film usually contains a unreacted PbI_2 at the interface between an electron transport layer (ETL) and a perovskite active layer. To reduce the unreacted PbI_2 in the 2-step prepared $MAPbI_3$ film, we have recently reported a new 3-step method, which was realized by an additional MA(I,Br) spin-coating. Here, we propose an advanced 3-step method, *viz.*, an additional $HC(NH_2)_2I$ (FAI) spin-coating on the 2-step prepared $MAPbI_3$ film. The additional FAI spin-coating formed a FA_xMA_{1-}

$_x$PbI$_3$ solid-solution by the incorporation of FA ion into MAPbI$_3$. Also, the additional FAI spin-coating yielded a FA$_y$MA$_{1-y}$PbI$_3$ layer (y>x) by converting the unreacted PbI$_2$, which resulted in the layered structure with different FA concentrations, and hence, with the multiple bandgap structure. The best PCE of 18.1% was achieved by optimizing the FAI spin-coating process.

KEYWORDS

perovskite solar cells, PbI$_2$, additional FAI spin-coating, FA$_x$MA$_{1-x}$PbI$_3$, multiple bandgap structure

1. INTRODUCTION

Perovskite solar cells have widely studied due to their high power conversion efficiency (PCE) and their easy production process. In the first report of perovskite solar cell in 2009, CH$_3$NH$_3$PbI$_3$ (MAPbI$_3$) and CH$_3$NH$_3$PbBr$_3$ (MAPbBr$_3$) were used as perovskite active layers.[1] Recently, mixed cations of CH$_3$NH$_3^+$ (MA), HC(NH$_2$)$_2^+$ (FA) and Cs$^+$ for the A site in ABX$_3$ have attracted much attention to obtain a high PCE of over 20%.[2-6] MAPbI$_3$ (~1.5-1.6 eV, [3,7] dark brawn color), α-FAPbI$_3$ (~1.48 eV,[3] black color) and α-CsPbI$_3$ (~1.73 eV[4]) have different bandgaps due to the differences of MA, FA and Cs ionic radii. Therefore, mixing these cations enables to control the bandgap of the perovskite active layer. In addition, the mixed cation structure improves the durability of perovskite solar cells.[2-6] Meanwhile, Cho et al. [8] and Kim et al. [9] reported that the anionic gradient structures with different I-Br concentrations in the vertical (thickness) direction effectively improved the carrier extraction and suppressed the carrier recombination due to the bandgap-gradient structures in the perovskite active layers.[8,9]

Various preparation methods of the perovskite active layer have also been developed to improve the solar cell performance.[10-17] Conventional preparation methods are usually categorized into the 1-step and the 2-step methods. In the typical 1-step method, the mixture of PbI_2 and CH_3NH_3I (MAI) is coated on the electron transport layer (ETL) and is converted to $MAPbI_3$ via the evaporation of solvent. In the typical 2-step method, a PbI_2 film is firstly prepared (by coating, depositing, etc.) and then it reacts with MAI to form $MAPbI_3$.

The 2-step method is relatively easy to control the morphology of perovskite active layer,[18] but unreacted PbI_2 usually remains at the interface of the ETL and the perovskite active layer. To solve this problem, some improved processes were proposed, *e.g.*, solvent selection and PbI_2 morphology control.[19-21] Instead of a conventional N,N-dimethylformamide (DMF) solvent, dimethyl sulfoxide (DMSO) effectively suppressed the crystallization of PbI_2 via the complex formation.[19,20] Another strategy is to form a porous PbI_2 film using a molecular level pore-forming agent, which is effective to increase the reactivity between PbI_2 and MAI.[21] Recently, we have reported an alternative method, *viz*. the 3-step method, to reduce the unreacted PbI_2, which is realized by the additional MA(I,Br) spin-coating.[22] The 3-step method resulted in the obvious enhancement of the PCE from 12.9% (2-step) to 14.4% (3-step) and of the stability in air.

Here, we propose further advanced 3-step method, *viz.*, additional 'FAI' spin-coating on the 2-step prepared $MAPbI_3$ film instead of the additional MAI on $MAPbI_3$ (**Figure 1**). The additional FAI spin-coating formed a $FA_xMA_{1-x}PbI_3$ solid-solution by the incorporation of FA ion into $MAPbI_3$. Also, the additional FAI spin-coating yielded a $FA_yMA_{1-y}PbI_3$ layer ($y>x$) by converting the unreacted PbI_2 at the interface of the ETL and the perovskite active layer,[23] which resulted in the multiple bandgap structure. The best PCE of 18.1% was achieved by optimizing the FAI spin-coating process.

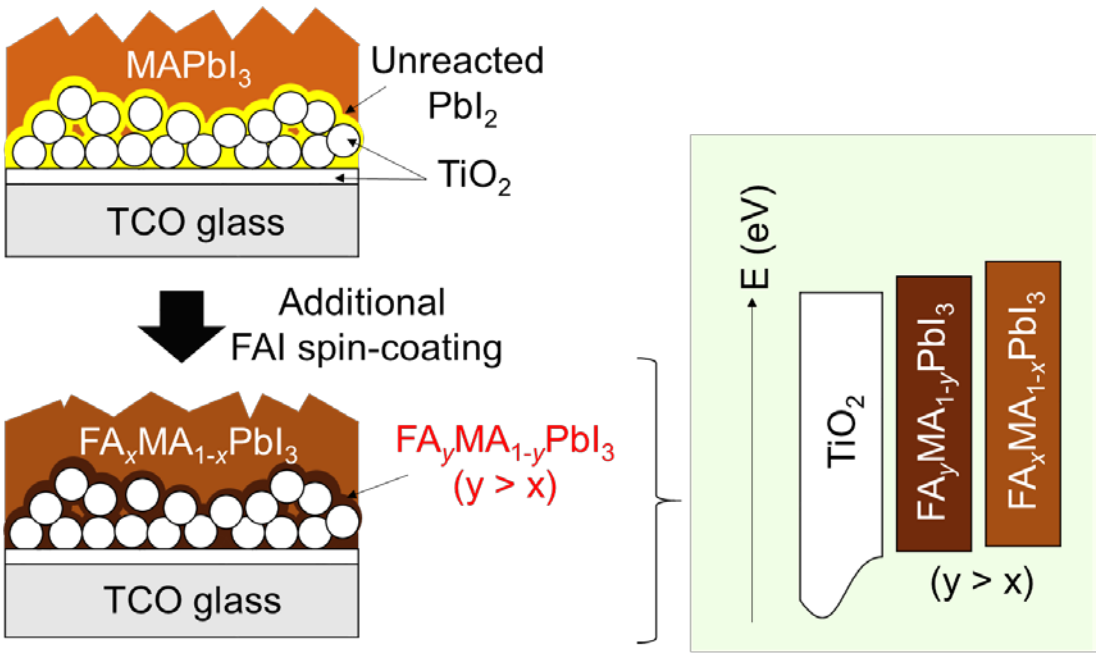

Figure 1. Design concept of the advanced 3-step method using additional FAI spin-coating on the 2-step prepared $MAPbI_3$ film, resulting in the multiple bandgap structure.

2. EXPERIMENTAL SECTION

2.1. Preparation of TiO_2 compact and mesoporous layers

Transparent conductive oxide (TCO, Type-0052, 10 Ω/sq., Geomatec) substrates were patterned by etching with Zn powder (>96.0%, Tokyo Chemical Industry) and 1 M HCl (Wako Pure Chemical Industry). Then, the substrates were cleaned by the ultrasonication in ethanol for 5 min and dried in air. The TiO_2 compact layers were prepared by spray-pyrolysis method; a solution of titanium diisopropoxide bis(acetylacetonate) (TAA, 75 wt% in isopropanol, Sigma-Aldrich) mixed in ethanol at the volume ratio of TAA:ethanol=2:25 was sprayed on the patterned substrates at 500 °C. TiO_2 mesoporous layers were then prepared by spin-coating a TiO_2 paste (18NR-T, Dyesol), diluted in ethanol at the weight ratio of TiO_2 paste:ethanol=1:5, on the

substrates at 4000 rpm for 25 s and by annealing at 500 °C for 30 min. Then, the substrates were exposed to ultraviolet light for 1 night in order to improve the contact with the PbI_2 solution in the next section.

2.2. Preparation of perovskite active layer, hole transport layer and metal electrode

The perovskite active layers and the hole transport layers (HTLs) were prepared in air with humidity of ~30%. The TiO_2 coated substrates were pre-heated at 60 °C. A 1 M solution of PbI_2 (>98.0%, Tokyo Chemical Industry) in DMF (99.5%, Nacalai tesque) was also pre-heated at 60 °C. The PbI_2 solution was then spin-coated on the substrates at 3000 pm for 20 s. After annealing at 60 °C for 10 min, the substrates were dipped in a 10 mg mL^{-1} solution of MAI (98%, Wako Pure Chemical Industry) dissolved in isopropanol (99.5%, Nacalai tesque) for 20 s, followed by rinsing with isopropanol and by annealing at 60 °C for 10 min. Then, 20 μL of MAI solution (0.13 M: 20 mg/mL) or FAI (≥98%, Sigma-Aldrich) solution of three concentrations (0.06 M: 10.8 mg/mL, 0.13 M: 21.6 mg/mL and 0.19 M: 32.4 mg/mL) was dropped on the prepared $MAPbI_3$ films during the spinning at 4000 rpm.

After annealing at 60 °C for 10 min, the HTLs with the thickness of ~200 nm were prepared by spin-coating a spiro-MeOTAD solution at 4000 rpm for 35 s. The spiro-MeOTAD solution in 1 mL chlorobenzene (99%, Nacalai tesque) was composed of 73 mg spiro-MeOTAD (99%, Sigma-Aldrich), 28.8 μL 4-*tert*-butylpyridine (TBP, 96.0%, Sigma-Aldrich) and 17 μL solution of [520 mg/mL lithium bis(trifluoromethylsulphonyl)imide salt (>98.0%, Tokyo Chemical Industry) in acetonitrile (99.5%, Wako Pure Chemical Industry)]. Finally, Ag electrodes with the thickness of ~50 nm were deposited on the HTLs with a thermal evaporator under the pressure of 3×10^{-5} Torr.

Hereinafter, we denotes the solar cells with 0.13 M additional MAI spin-coating as MAI: 0.13 M and those with additional 0.06 M, 0.13 M and 0.19 M FAI spin-coating as FAI: 0.06 M, FAI: 0.13 M and FAI: 0.19 M, respectively.

2.3. Characterizations

Crystal structures of the prepared perovskite active layers on ETL were characterized by X-ray diffraction (XRD, Multiflex, Cu-K_{α}, 40 kV and 40 mA, Rigaku). Their optical absorbance and transmittance were measured by the ultraviolet-visible absorption spectroscopy (UV-Vis, UV-1280, Shimadzu). Steady-state photoluminescence (PL) was measured using a Ramascope System1000 (Renishaw) with an excitation laser of wavelength 325 nm (IK5651R-G, Kimmon). The top-view and cross-section microstructures of perovskite active layers on ETL were observed by scanning electron microscopy (SEM, SU-8020, Hitachi High-technologies). The chemical composition of the surface of perovskite active layers were measured by SEM (TM3000, Hitachi, operated at 15 kV) equipped with energy dispersive X-ray spectrometry (EDS). Current density-voltage (*J-V*) characteristics were measured using a solar simulator (XES-40S1, SAN-EI Electric), which was calibrated to AM 1.5, 100 mW/cm^2 with a standard silicon photodiode (BS-520BK, Bunkoukeiki). The *J-V* curves were measured by reverse (1.1V → 0V) and forward (0V → 1.1V) scans. The voltage step and delay time were 20 mV and 50 ms, respectively. The cell size was 1.25×1.25 cm^2, and the active area was limited to 0.084 cm^2 by using a black mask. Monochromatic incident photon-to-current conversion efficiency (IPCE) spectra were measured in direct current mode (SM-250, Bunkoukeiki).

3. RESULTS AND DISCUSSION

3.1. Phase analysis

Figure 2 shows XRD patterns of perovskite active layers on ETL prepared by the 2-step and the 3-step methods including additional MAI or FAI spin-coating. The peaks in the 2-step sample well corresponded to $MAPbI_3$ and unreacted PbI_2 (a relatively large peak at 2θ=~12.8°). For the 3-step samples, the peak intensity of unreacted PbI_2 significantly decreased due to a conversion of the unreacted PbI_2, similarly to our previous work.[22] Although a small peak of unreacted PbI_2 at ~12.8° still remained in the 3-step films, the peak intensity effectively decreased with increasing the FAI concentration. Furthermore, the peaks for the perovskite shifted to smaller angles by the additional FAI spin-coating, and the peak shift became larger with increasing the FAI concentration as seen in the enlarged XRD patterns at 13°-15°. These results indicate that the additional FAI spin-coating yielded $FA_xMA_{1-x}PbI_3$, and that the x value in $FA_xMA_{1-x}PbI_3$ became larger with increasing the FAI concentration.[2]

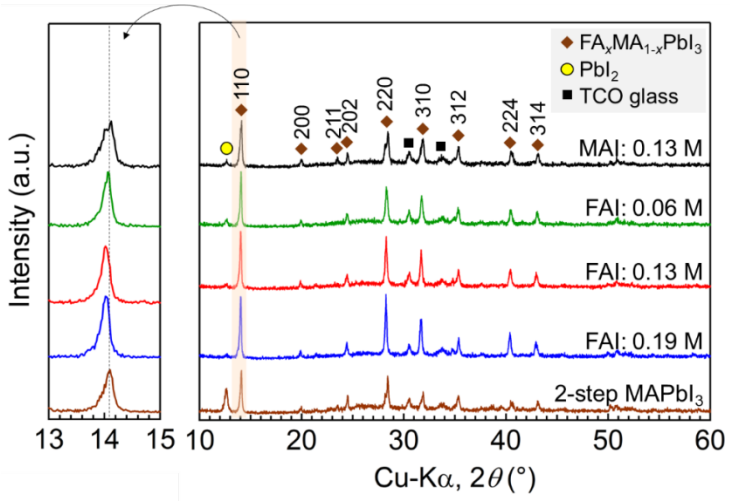

Figure 2. XRD patterns of perovskite active layers on ETL prepared by the 2-step and the 3-step methods including additional MAI or FAI spin-coating.

3.2. Optical properties

Figure 3a shows the absorbance spectra of the 3-step prepared perovskite active layers on ETL. The wavelengths of absorption edges for FAI spin-coated cells were longer than that for MAI: 0.13 M (~780 nm). The bandgaps were estimated from the Tauc plot of the absorption edge calculated from **Figure 3a**. The bandgap of MAI: 0.13 M was ~1.61 eV, which was comparable to the reported bandgap of $MAPbI_3$ (~1.55-1.6 eV).[3,7] The bandgap of FAI: 0.06 M, 0.13 M and 0.19 M were ~1.59 eV, 1.58 eV and 1.57 eV, respectively; it became smaller with increasing the FAI concentration. These results also indicate the increase of *x* value in the $FA_xMA_{1-x}PbI_3$ with increasing the FAI concentration, since the bandgap of α-$FAPbI_3$ (~1.48 eV)[3] is smaller than that of $MAPbI_3$. **Figure 3b** shows the transmittance spectra of the 3-step prepared perovskite active layers on ETL. The transmittances of the additionally FAI spin-coated perovskite active layers were smaller than that of MAI: 0.13 M at >650 nm, which indicates better light absorption.

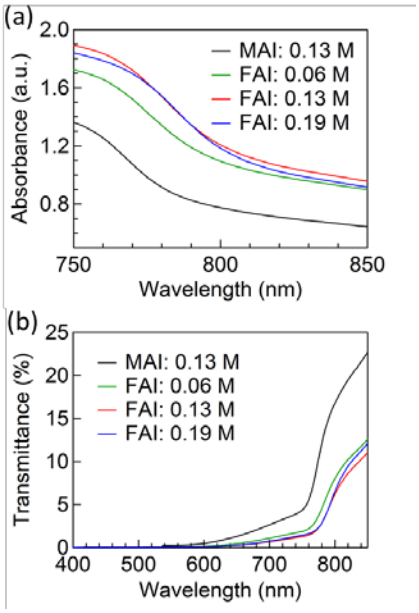

Figure 3. (a) Absorbance and (b) transmittance spectra of the 3-step prepared perovskite active layers on ETL.

3.3. Layered structure with different FA concentrations

Now we focus on the layered structure with different FA concentrations (**Figure 1**). The unreacted PbI_2 (thickness of several tens nanometer) is reported to exist mainly at the interface between ETL and perovskite active layer.[23] The additional FAI spin-coating converted $MAPbI_3$ into $FA_xMA_{1-x}PbI_3$ (as shown in **Figure 2**) and it should also convert the unreacted PbI_2 into $FA_yMA_{1-y}PbI_3$ (y>x) (not directly detected in **Figure 2**). This layered structure should produce the multiple bandgap structure as illustrated in **Figure 1**.

To detect the different bandgaps of the 'XRD-invisible' multilayer structure, we measured the PL spectra of perovskite active layers from the top and back substrate sides. The substrate used in this section was a commercial slide glass plate (No. 10005000, Marienfeld), and He-Cd laser of the wavelength of 325 nm was used to excite the perovskite active layer. The penetration depth of the laser in the $(FA,MA)PbI_3$ active layer was estimated to be ~20-25 nm, judging from inverses of absorption coefficients of $MAPbI_3$ and $FAPbI_3$ at the wavelength of 325 nm (α=~4-5×10^7 m^{-1}),[24] which is sufficiently thin to evaluate the expected $FA_yMA_{1-y}PbI_3$ layer.

Figure 4 shows the normalized PL spectra of perovskite active layers on ETL for MAI: 0.13 M and FAI: 0.19 M. When the laser was eradiated from the top side, MAI: 0.13 M and FAI: 0.19 M showed the PL peaks at ~775 nm and ~788 nm, respectively. These values are in good agreements with their estimated bandgaps. On the other hand, when the laser was eradiated from the back substrate side, FAI: 0.19 M only showed a large peak shift to ~800 nm and somewhat asymmetric peak shape. These results strongly suggest that (1) FAI: 0.19 M was mainly composed of $FA_xMA_{1-x}PbI_3$ (bandgap of 1.57 eV), and (2) the thin $FA_yMA_{1-y}PbI_3$ layer (bandgap of ~1.55 eV) existed at the interface of ETL and perovskite active layer. This multiple bandgap structure (through the layered structure with different FA concentrations) must be effective to suppress the carrier recombination and improve the solar cell performance, similarly to the bandgap gradient (through the anion concentration gradient) in the literature.[8,9]

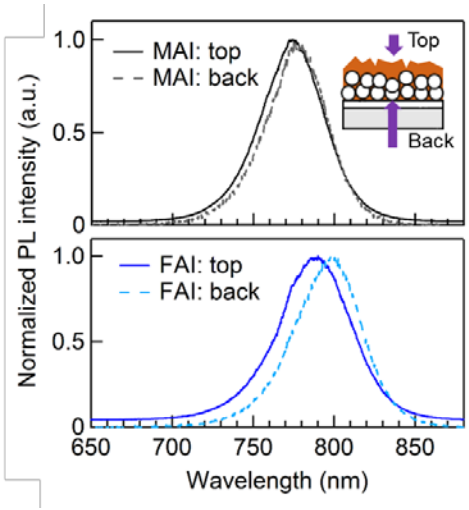

Figure 4. PL spectra of the perovskite active layers on ETL for MAI: 0.13 M and FAI: 0.19 M measured from perovskite top side and back substrate side.

3.4. Morphology of perovskite active layer

Figures 5a-d show top-view SEM images of the 3-step prepared perovskite active layers on ETL. The perovskite particles with the diameter of ~0.5-1 μm were observed in all the samples. As we reported in the previous study,[22] some bridge-like networks between perovskite particles were observed in MAI: 0.13 M, which were formed by the surface dissolution of perovskite particles during the additional spin-coating (see also **Figure S1** as enlargement). On the other hand, the bridge-like networks were not frequently observed in the additionally FAI spin-coated cells. Instead, the grain boundaries became unclear (i.e. intergranular voids were filled) and small pores at the surface of perovskite particles were observed, especially in FAI: 0.19 M. These morphological changes for the FAI samples are also attributable to the surface dissolution of perovskite particle despite the different morphology from MAI: 0.13 M.

Figures 5e-h show cross-sectional SEM images of the 3-step prepared perovskite active layers on ETL. All the cells had comparable thicknesses of the TiO_2 mesoporous/perovskite

layers (totally ~150 nm) and the perovskite capping layers (~500 nm). The grain boundaries became unclear with increasing the FAI concentration (**Figures 5f-h**), which is in good agreement with the top-view SEM images.

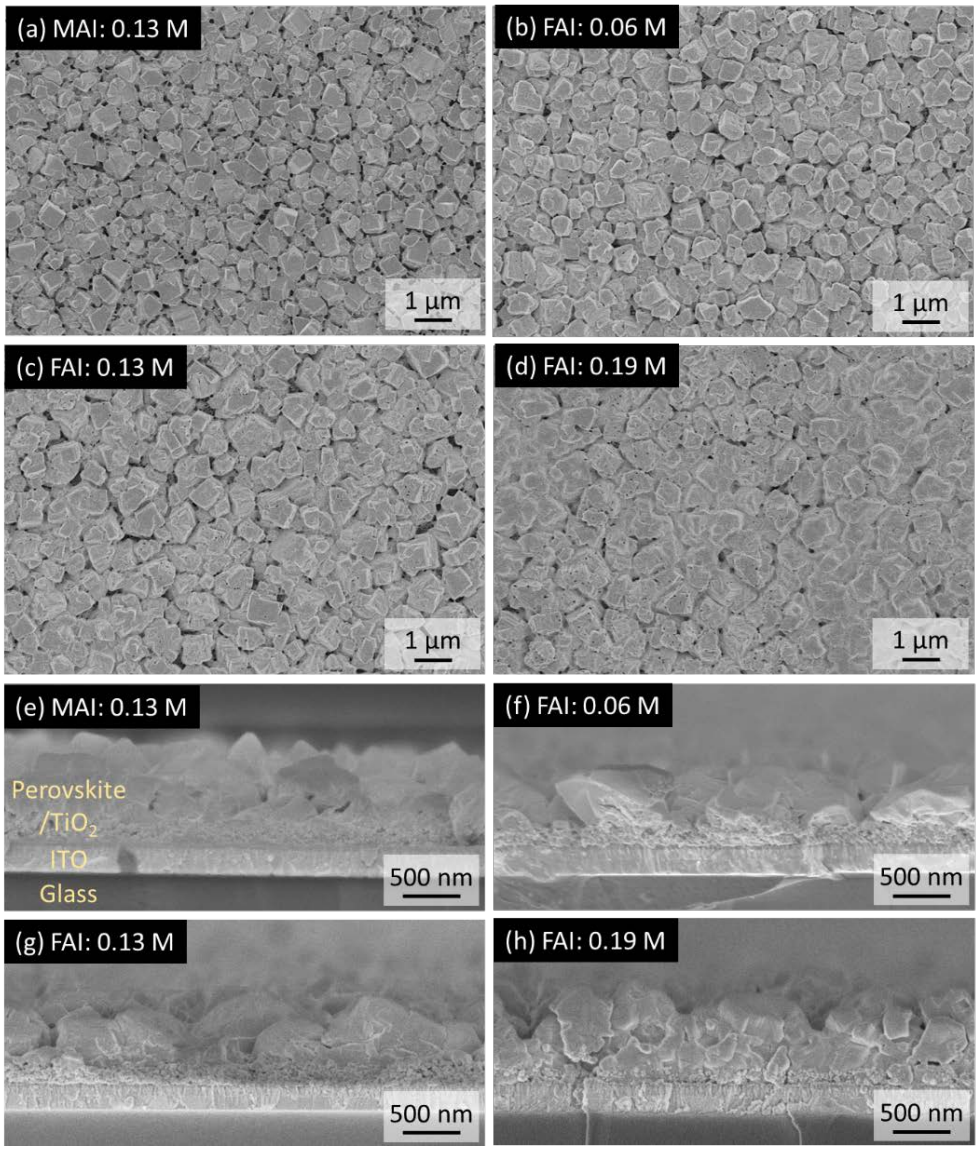

Figure 5. (a)-(d) Top-view and (e)-(h) cross-sectional SEM images of the 3-step prepared perovskite active layers on ETL.

3.5. Photovoltaic performance

Table 1 and **Figure 6a** show *J-V* characteristics and *J-V* curves of the 3-step prepared solar cells (reverse scan), respectively. The values in the table are average of 10 devices for FAI: 0.19 M and 15 devices for others. MAI: 0.13 M showed *J*sc of 23.5 mA/cm^2, *V*oc of 971 mV, fill factor (*FF*) of 0.71 and PCE of 16.3%, whereas FAI: 0.13 M had *J*sc of 24.1 mA/cm^2, V_{OC} of 962 mV, *FF* of 0.73 and PCE of 16.8%. Therefore FAI: 0.13 M showed 0.5 point (3.1%) higher efficiency than MAI: 0.13 M.

To clarify the reason of the improved J_{SC} of FAI: 0.13 M cell compared with MAI: 0.13 M cell, IPCE spectra were measured (**Figure 6b**). The IPCE spectrum of FAI: 0.13 M was shifted to longer wavelength than that of MAI: 0.13 M due to its smaller bandgap, and this shift contributed to the larger *J*sc. The slight decrease of V_{OC} in FAI: 0.13 M can be also ascribed to its smaller bandgap. The V_{OC} and bandgap generally have positive correlation; for example, an increase of bandgap by incorporating Br into $MAPbI_3$ perovskite active layer ($MAPbI_3 \rightarrow MAPbI_{3-x}Br_x$) generated larger V_{OC}.[7,25]

As for the effect of FAI concentration on *J*sc, the *J*sc increased from 23.4 mA/cm^2 to 24.1 mA/cm^2, and then decreased to 23.5 mA/cm^2 by increasing the FAI concentration from 0.06 M, 0.13 M to 0.19 M (**Table 1**). The increase in J_{SC} (FAI: 0.06→0.13 M) is attributable to the higher conversion from unreacted PbI_2 into perovskite, which gives better light absorption. While, the decrease in J_{SC} (FAI: 0.13→0.19 M) may be attributable to the excess FAI remained at grain boundaries and surfaces, particularly in FAI: 0.19 M. Indeed, the IPCE spectrum of FAI: 0.19 M was smaller than that of FAI: 0.13 M in spite of their comparable absorbance spectra (**Figure 3a**). Furthermore, some of the prepared cells showed the abnormal behavior of large current drop around J_{SC}, especially for FAI: 0.19 M, as shown in **Figure S2** due to the excess FAI on the surface of the perovskite active layer. The *J-V* characteristics of these cells are not included in the averaged photovoltaic performance because their *FF* values are incorrect.

As for the effect of FAI concentration on V_{OC}, the V_{OC} increased from 951 mV to 962 mV, and again increased to 989 mV by increasing the FAI concentration from 0.06 M, 0.13 M to 0.19 M (**Table 1**), despite the decreased bandgaps (~1.59 eV, 1.58 eV and 1.57 eV). This V_{OC} enhancement can be attributed to (1) the decrease of unreacted PbI_2, (2) the decrease of grain boundary, and (3) the suppression of carrier recombination by the multiple bandgap structure.[8,9]

Table 1. *J-V* characteristics of the 3-step prepared solar cells (reverse scan). The values are average of 10 devices for FAI: 0.19 M and 15 devices for others.

Samples	J_{SC} (mA/cm^2)	V_{OC} (mV)	*FF*	PCE (%)
MAI: 0.13 M	23.5	971	0.71	16.3
FAI: 0.06 M	23.4	951	0.70	15.5
FAI: 0.13 M	24.1	962	0.73	16.8
FAI: 0.19 M	23.5	989	0.73	17.0

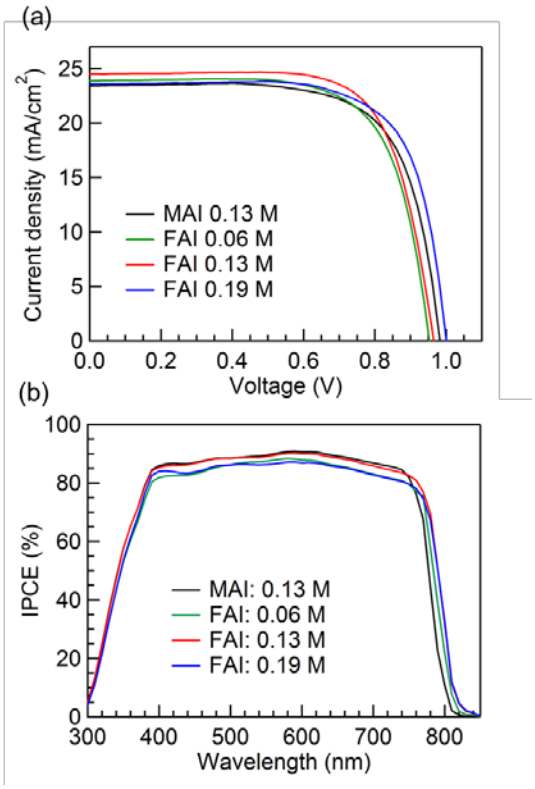

Figure 6. (a) *J-V* curves (reverse scan) and (b) IPCE spectra of the 3-step prepared solar cells.

3.6. Effect of the excess FAI at the surface

To verify the assumption in section 3.5 (i.e. excess FAI existed in FAI: 0.19 M), we measured the atomic ratio of I (iodide) and Pb (lead) at the surface of perovskite active layer ($FA_xMA_{1-x}PbI_3$) by EDS as shown in **Figure 7.** If the excess FAI ($HC(NH_2)_2I$) exists on the surface of $FA_xMA_{1-x}PbI_3$, the atomic ratio of iodide must increase and that of lead must decrease. Actually, the atomic ratio of iodide increased and that of lead decreased with increasing the FAI concentration of the additional spin-coating solutions. This result supported the assumption of the excess FAI. To remove the excess FAI, the FAI: 0.19 M sample was rinsed with isopropanol (IPA) and annealed for 10 min after the additional spin-coating process. The atomic ratio of iodide became smaller after the IPA rinsing, which suggests the removal of the excess FAI.

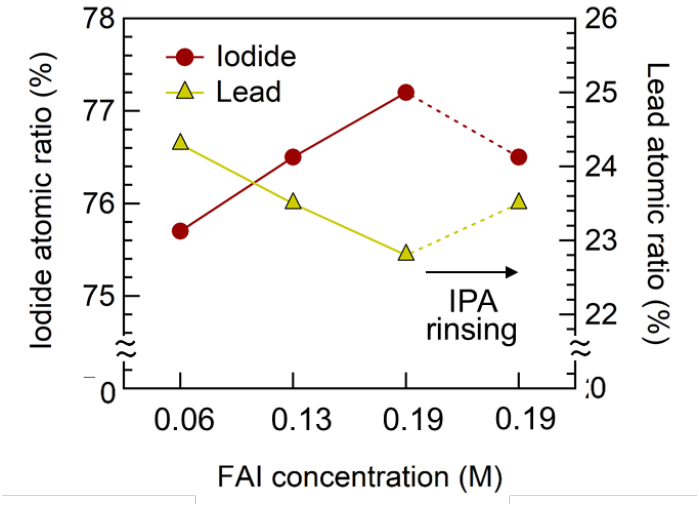

Figure 7. Atomic ratio of iodide and lead at the surface of the perovskite active layers for the additionally FAI spin-coated cells.

The *J-V* characteristics (reverse scan, average of 15 devices) of the IPA-rinsed cells are shown in **Table 2**. Although the V_{OC} slightly decreased compared with that without rinsing, the J_{SC} was increased up to 24.4 mA/cm^2, and the largest PCE (average) of 17.2% in this study was obtained. Moreover, the current drop behavior around J_{SC} was not observed for the IPA-rinsed cells. **Figure 8** shows the *J-V* curve of the best performance cell (reverse scan, non-average) with the maximum PCE of 18.1%.

Table 2. *J-V* characteristics (reverse scan) of FAI: 0.19 M with isopropanol rinsing and 10 min annealing after the additional spin-coating process. The values are average of 15 devices.

Sample	J_{SC} (mA/cm^2)	V_{OC} (mV)	*FF*	PCE (%)
FAI: 0.19 M with IPA rinsing	24.4	970	0.73	17.2

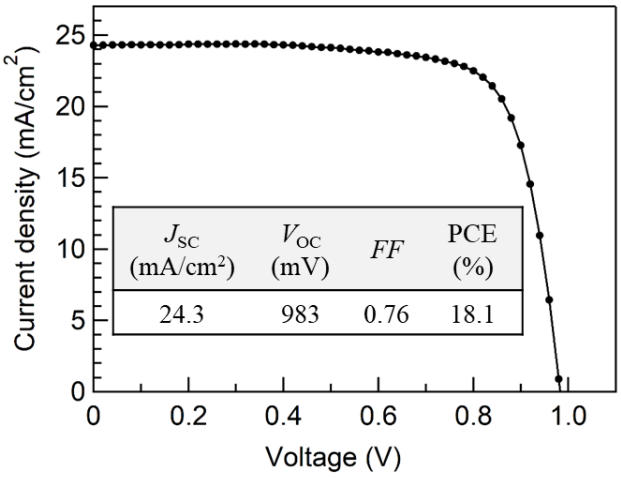

Figure 8. The *J-V* curve and characteristics (reverse scan) of the best performance cell: FAI: 0.19 M with isopropanol rinsing and 10 min annealing after the additional spin-coating process.

4. CONCLUSIONS

In this study, we proposed an advanced 3-step method, *viz.*, additional FAI spin-coating on the 2-step prepared $MAPbI_3$ film instead of additional MAI on $MAPbI_3$. In conclusions:

(1) The 3-step cells prepared by the additional FAI spin-coating had the smaller bandgaps than the 3-step cell by the additional MAI, due to the formation of $FA_xMA_{1-x}PbI_3$. Moreover, the layered structure (or maybe "gradient" structure) with different FA concentrations was also generated in the FAI cells by converting the unreacted PbI_2 into $FA_yMA_{1-y}PbI_3$ at the interface between ETL and perovskite active layer, which resulted in the multiple bandgap structure.

(2) The 3-step FAI cells had increased J_{SC} (24.1 mA/cm^2) and slightly decreased V_{OC} (962 mV) compared with the 3-step MAI cell, due to the smaller bandgap of FAI cells. As a result, the larger PCEs (average) of 16.8% and 17.0 % were obtained for FAI: 0.13 M and 0.19 M, respectively.

(3) The increase of FAI concentration in the spin-coated solution was effective to increase J_{SC} up to 0.13 M due to the effective PbI_2 conversion, but the much higher concentration of FAI (0.19 M) decreased J_{SC} due to the excess FAI remained at the grain boundaries and surfaces. The increase of FAI concentration monotonically improved V_{OC} due to the decrease of unreacted PbI_2, decrease of grain boundary, and suppression of carrier recombination by the multiple bandgap structure. The best PCE of 18.1% was achieved by optimizing the additional FAI spin-coating process.

ASSOCIATED CONTENT

Supporting Information

The following files are available free of charge.

Enlarged top-view SEM images of MAI: 0.13 M and FAI: 0.13 M (**Figure S1**); *J-V* curve with current drop around J_{SC} (**Figure S2**); Effect of annealing temperature including box plots of *J-V* characteristics of MAI: 0.13 M and FAI: 0.13 M and XRD patterns of MAI: 0.13 M annealed at 60, 100 and 150 °C (**Figures S3, S4 and S5**) (PDF)

AUTHOR INFORMATION

Corresponding Author

* E-mail: suzuki@ims.tsukuba.ac.jp

Author Contributions

The manuscript was written by Yuji Okamoto and Yoshikazu Suzuki. PL and IPCE measurements were supported by Takeshi Yasuda and Masatomo Sumiya.

Notes

The authors declare no competing financial interest.

ACKNOWLEDGMENT

We thank Research Facility Center for Science and Technology, University of Tsukuba, and Dr. T. S. Suzuki at NIMS for the use of SEM.

REFERENCES

(1) Kojima, A.; Teshima, K.; Shirai, Y.; Miyasaka, T. Organometal Halide Perovskites as Visible-Light Sensitizers for Photovoltaic Cells. *J. Am.Chem. Soc.* **2009**, 131, 6050–6051.

(2) Pellet, N.; Gao, P.; Gregori, G.; Yang, T. Y.; Nazeeruddin, M. K.; Maier, J.; Gra□tzel, M. Mixed-Organic-Cation Perovskite Photovoltaics for Enhanced Solar-Light Harvesting. *Angew. Chem. Int. Ed.* **2014**, 53, 3151–3157.

(3) Jeon, N. J.; Noh, J. H.; Yang, W. S.; Kim, Y. C.; Ryu, S.; Seo, J.; Seok, S. I. Compositional Engineering of Perovskite Materials for High-Performance Solar Cells. *Nature* **2015**, 517, 476–480.

(4) Saliba, M.; Matsui, T.; Seo, J. Y.; Domanski, K.; Correa- Baena, J. P.; Nazeeruddin, M. K.; Zakeeruddin, S. M.; Tress, W.; Abate, A.; Hagfeldt, A.; Grätzel, M. Cesium-Containing Triple Cation Perovskite Solar Cells: Improved Stability, Reproducibility and High Efficiency. *Energy Environ. Sci.* **2016**, 9, 1989–1997.

(5) Yang, W. S.; Park, B. W.; Jung, E. H.; Jeon, N. J.; Kim, Y. C.; Lee, D. U.; Shin, S. S.; Seo, J.; Kim, E. K.; Noh, J. H.; Seok, S. I. Iodide Management in Formamidinium-Lead-Halide–Based Perovskite Layers for Efficient Solar Cells. *Science* **2017**, 356, 1376–1379.

(6) Saliba, M.; Matsui. T.; Domanski, K.; Seo, J. Y.; Ummadisingu, A.; Zakeeruddin, S. M.; Correa-Baena, J. P.; Tress, W. R.; Abate, A.; Hagfeldt, A.; Grätzel, M. Incorporation of Rubidium Cations into Perovskite Solar Cells Improves Photovoltaic Performance. *Science* **2016**, 354, 206–209.

(7) Noh, J. H.; Im, S. H.; Heo, J. H.; Mandal. T. N.; Seok, S. I. Chemical Management for Colorful, Efficient, and Stable Inorganic-Organic Hybrid Nanostructured Solar Cells. *Nano Lett.* **2013**, 13, 1764−1769.

(8) Cho, K. T.; Paek, S.; Grancini, G.; Rolda´n-Carmona, C.; Gao, P.; Lee, Y.; Nazeeruddin, M. K. Highly Efficient Perovskite Solar Cells with a Compositionally Engineered Perovskite/Hole Transporting Material Interface. *Energy Environ. Sci.* **2017**, 10, 621–627.

(9) Kim, M; Kim, B. J.; Son, D. Y.; Park, N. G.; Jung, H. S.; Choi, M. Observation of Enhanced Hole Extraction in Br Concentration Gradient Perovskite Materials. *Nano Lett.* **2016**, 16, 5756−5763.

(10) Liu, M.; Johnston, M. B.; Snaith, H. J. Efficient Planar Heterojunction Perovskite Solar Cells by Vapour Deposition. *Nature* **2013**, 501, 395−398.

(11) Burschka, J.; Pellet, N.; Moon, S. J.; Humphry-Baker, R.; Gao, P.; Nazeeruddin, M. K.; Grätzel, M. Sequential Deposition as a Route to High-Performance Perovskite-Sensitized Solar Cells. *Nature* **2013**, 499, 316–319.

(12) Chen, Q.; Zhou, H.; Hong, Z.; Luo, S.; Duan, H. S.; Wang, H. H.; Liu, Y.; Li, G.; Yang, Y. Planar Heterojunction Perovskite Solar Cells via Vapor-Assisted Solution Process. *J. Am. Chem. Soc.* **2014**, 136, 622−625.

(13) Xiao, Z.; Dong, Q.; Bi, C.; Shao, Y.; Yuan, Y.; Huang, J. Solvent Annealing of Perovskite-Induced Crystal Growth for Photovoltaic-Device Efficiency Enhancement. *Adv. Mater.* **2014**, 26, 6503–6509.

(14) Jeon, N. J.; Noh, J. H.; Kim, Y. C.; Yang, W. S.; Ryu, S.; Seok, S. I. Solvent Engineering for High-Performance Inorganic–Organic Hybrid Perovskite Solar Cells. *Nat. Mate*r. **2014**, 13, 897–903.

(15) Xiao, M.; Huang, F.; Huang, W.; Dkhissi, Y.; Zhu, Y.; Etheridge, J.; Gray-Weale, A.; Bach, U.; Cheng, Y. B. Spiccia, L. A Fast Deposition-Crystallization Procedure for Highly Efficient Lead Iodide Perovskite Thin-Film Solar Cells. *Angew. Chem. Int. Ed.* **2014**, 53, 9898–9903.

(16) Nie, W.; Tsai, H.; Blancon, J. C.; Asadpour, R.; Blancon, J. C.; Neukirch, A. J.; Gupta, G.; Crochet, J. J.; Chhowalla, M.; Tretiak, S.; Alam, M. A.; Wang, H. L.; Mohite, A. D. High-Efficiency Solution-Processed Perovskite Solar Cells with Millimeter-Scale Grains. *Science* **2015**, 347, 522–525.

(17) Li, X.; Bi, D.; Yi, C.; Décoppet, J. D.; Luo, J.; Zakeeruddin, S. M.; Hagfeldt, A.; Grätzel, M. A Vacuum Flash-Assisted Solution Process for High-Efficiency Large-Area Perovskite Solar Cells. *Science* **2016**, 353, 58–62.

(18) Im, J. H.; Kim, H. S.; Park, N. G. Morphology-Photovoltaic Property Correlation in Perovskite Solar Cells: One-Step versus Two-Step Deposition of $CH_3NH_3PbI_3$. *APL Mater.* **2014**, 2, 081510.

(19) Li, W.; Fan, J.; Li, J.; Mai, Y.; Wang, L. Controllable Grain Morphology of Perovskite Absorber Film by Molecular Self-Assembly toward Efficient Solar Cell Exceeding 17%, *J. Am. Chem. Soc.* **2015**, 137, 10399−10405.

(20) Wu, Y.; Islam, A.; Yang, X.; Qin, C.; Liu, J.; Zhang, K.; Penga W.; Han, L. Retarding the Crystallization of PbI_2 for Highly Reproducible Planar-Structured Perovskite Solar Cells via Sequential Deposition. *Energy Environ. Sci.* **2014**, 7, 2934–2938.

(21) Cao, J.; Wang, F.; Yu, H.; Zhou, Y.; Lu, H.; Zhao, N.; Wong, C. P. Porous PbI_2 Films for the Fabrication of Efficient, Stable Perovskite Solar Cells via Sequential Deposition. *J. Mater. Chem. A* **2016**, 4, 10223–10230.

(22) Okamoto, Y.; Suzuki, Y. Perovskite Solar Cells Prepared by a New 3-Step Method Including a PbI_2 Scavenging Step. *Mater. Sci. Semicond. Process.* **2017**, 71, 1–6.

(23) Kim, S. Y.; Jo, H. J.; Sung, S. J.; Kim, D. H. Perspective: Understanding of Ripening Growth Model for Minimum Residual PbI_2 and its Limitation in the Planar Perovskite Solar Cells. *APL Mater.* **2016**, 4, 100901.

(24) Xie, Z.; Sun, S.; Yan, Y.; Zhang, L.; Hou, R.; Tian, F.; Qin, G. G. Refractive Index and Extinction Coefficient of $NH_2CH = NH_2PbI_3$ Perovskite Photovoltaic Material. *J. Phys.: Condens. Matter.* **2017,** 29, 245702.

(25) Zhu, W.; Bao, C.; Li, F.; Yu, T.; Gao, H.; Yi, Y.; Yang, J.; Fu, G.; Zhou, X.; Zou, Z. A Halide Exchange Engineering for $CH_3NH_3PbI_{3-x}Br_x$ Perovskite Solar Cells with High Performance and Stability. *Nano energy* **2016**, 19, 17−26.

GRAPHICAL ABSTRACT